

Time-delay to intensity mapping based on a second-order optical integrator: application to optical arbitrary waveform generation

Reza Ashrafi,^{1,*} Mohammad Rezagholipour Dizaji,¹ Luis Romero Cortés,² Jiejun Zhang,³ Jianping Yao,³ José Azaña,² and Lawrence R. Chen¹

¹Department of Electrical and Computer Engineering, McGill University, Montreal, QC H3A 0E9 Canada

²Institut National de la Recherche Scientifique—Énergie, Matériaux et Télécommunications, Montréal, QC H5A1K6, Canada

³Microwave Photonics Research Laboratory, School of Electrical Engineering and Computer Science, University of Ottawa, Ontario K1N 6N5, Canada

*reza.ashrafi@mail.mcgill.ca

Abstract: We propose and validate experimentally a time-delay to intensity mapping process based on second-order optical integrators. This mapping provides dynamic control of the intensity modulation profile of a waveform based on a purely passive and linear process. In particular, we can realize linear intensity control by tuning the time-delay between two optical pulses launched into a second-order optical integrator. We suggest and experimentally prove the use of this mapping process for reconfigurable optical arbitrary waveform generation.

©2015 Optical Society of America

OCIS codes: (230.1150) All-optical devices; (070.1170) Analog optical signal processing; (320.5540) Pulse shaping; (070.7145) Ultrafast processing; (060.2340) Fiber optics components; (050.2770) Gratings.

References and links

1. K. Goda and B. Jalali, "Dispersive Fourier transformation for fast continuous single-shot measurements," *Nat. Photonics* **7**(2), 102–112 (2013).
2. H. Emami, N. Sarkhosh, L. A. Bui, and A. Mitchell, "Amplitude independent RF instantaneous frequency measurement system using photonic Hilbert transform," *Opt. Express* **16**(18), 13707–13712 (2008).
3. R. Ashrafi and J. Azaña, "Figure of merit for photonic differentiators," *Opt. Express* **20**(3), 2626–2639 (2012).
4. M. Ferrera, Y. Park, L. Razzari, B. E. Little, S. T. Chu, R. Morandotti, D. J. Moss, and J. Azaña, "On-chip CMOS-compatible all-optical integrator," *Nat. Commun.* **1**(29), 29 (2010).
5. S. Tan, Z. Wu, L. Lei, S. Hu, J. Dong, and X. Zhang, "All-optical computation system for solving differential equations based on optical intensity differentiator," *Opt. Express* **21**(6), 7008–7013 (2013).
6. N. Q. Ngo and L. N. Binh, "Optical realization of Newton-Cotes-based integrators for dark soliton generation," *J. Lightwave Technol.* **24**(1), 563–572 (2006).
7. M. T. Hill, H. J. S. Dorren, T. De Vries, X. J. M. Leijtens, J. H. Den Besten, B. Smalbrugge, Y.-S. Oei, H. Binsma, G.-D. Khoe, and M. K. Smit, "A fast low-power optical memory based on coupled micro-ring lasers," *Nature* **432**(7014), 206–209 (2004).
8. M. H. Asghari, C. Wang, J. Yao, and J. Azaña, "High-order passive photonic temporal integrators," *Opt. Lett.* **35**(8), 1191–1193 (2010).
9. M. Ferrera, Y. Park, L. Razzari, B. E. Little, S. T. Chu, R. Morandotti, D. J. Moss, and J. Azaña, "All-optical 1st and 2nd order integration on a chip," *Opt. Express* **19**(23), 23153–23161 (2011).
10. M. H. Asghari and J. Azaña, "Proposal for arbitrary-order temporal integration of ultrafast optical signals using a single uniform-period fiber Bragg grating," *Opt. Lett.* **33**(13), 1548–1550 (2008).
11. N. Huang, M. Li, R. Ashrafi, L. Wang, X. Wang, J. Azaña, and N. Zhu, "Active Fabry-Perot cavity for photonic temporal integrator with ultra-long operation time window," *Opt. Express* **22**(3), 3105–3116 (2014).
12. L. Lepetit, G. Chériaux, and M. Joffre, "Linear techniques of phase measurement by femtosecond spectral interferometry for applications in spectroscopy," *J. Opt. Soc. Am. B* **12**(12), 2467–2474 (1995).
13. Z. Jiang, D. E. Leaird, and A. M. Weiner, "Line-by-line pulse shaping control for optical arbitrary waveform generation," *Opt. Express* **13**(25), 10431–10439 (2005).
14. J. Chou, Y. Han, and B. Jalali, "Adaptive RF-photonic arbitrary waveform generator," *IEEE Photon. Technol. Lett.* **15**(4), 581–583 (2003).

15. S. T. Cundiff and A. M. Weiner, "Optical arbitrary waveform generation," *Nat. Photonics* **4**(11), 760–766 (2010).
16. Y. Park, M. H. Asghari, T. J. Ahn, and J. Azaña, "Transform-limited picosecond pulse shaping based on temporal coherence synthesis," *Opt. Express* **15**(15), 9584–9599 (2007).
17. V. Kaman, X. Zheng, R. J. Helkey, C. Pularla, and J. E. Bowers, "A 32-element 8-Bit photonic true-time-delay system based on a 288×288 3-D MEMS optical switch," *IEEE Photon. Technol. Lett.* **15**(6), 849–851 (2003).
18. D. B. Hunter, M. E. Parker, and J. L. Dexter, "Demonstration of a continuously variable true-time delay beamformer using a multichannel chirped fiber grating," *IEEE Trans. Microw. Theory Tech.* **54**(2), 861–867 (2006).
19. S. Blais and J. Yao, "Photonic true-time delay beamforming based on superstructured fiber Bragg gratings with linearly increasing equivalent chirps," *J. Lightwave Technol.* **27**(9), 1147–1154 (2009).
20. K. Horikawa, I. Ogawa, T. Kitoh, and H. Ogawa, "Silica-based integrated planar lightwave true-time-delay network for microwave antenna applications," in *Proceedings of the Optical Fiber Communication Conference*, (San Jose, Calif., 1996), **Vol. 2**, pp. 100–101.
21. B. Howley, X. Wang, M. Chen, and R. T. Chen, "Reconfigurable delay time polymer planar lightwave circuit for an X-band phased-array antenna demonstration," *J. Lightwave Technol.* **25**(3), 883–890 (2007).
22. Y. O. Barmenkov, J. L. Cruz, A. Díez, and M. V. Andrés, "Electrically tunable photonic true-time-delay line," *Opt. Express* **18**(17), 17859–17864 (2010).
23. X. Luo, H. Chen, and A. W. Poon, "Electro-optical tunable time delay and advance in silicon microring resonators," *Opt. Lett.* **35**(17), 2940–2942 (2010).
24. S. Khan, M. A. Baghban, and S. Fathpour, "Electrically tunable silicon photonic delay lines," *Opt. Express* **19**(12), 11780–11785 (2011).
25. S. Khan and S. Fathpour, "Complementary apodized grating waveguides for tunable optical delay lines," *Opt. Express* **20**(18), 19859–19867 (2012).
26. J. Xie, L. Zhou, Z. Zou, J. Wang, X. Li, and J. Chen, "Continuously tunable reflective-type optical delay lines using microring resonators," *Opt. Express* **22**(1), 817–823 (2014).
27. J. Xie, L. Zhou, Z. Li, J. Wang, and J. Chen, "Seven-bit reconfigurable optical true time delay line based on silicon integration," *Opt. Express* **22**(19), 22707–22715 (2014).
28. S. Yegnanarayanan, P. D. Trinh, F. Coppinger, and B. Jalali, "Compact silicon-based integrated optic time delays," *IEEE Photon. Technol. Lett.* **9**(5), 634–635 (1997).
29. <http://www.ll.mit.edu/about/facility-EPiF.html>
30. N. K. Fontaine, D. J. Geisler, R. P. Scott, T. He, J. P. Heritage, and S. J. B. Yoo, "Demonstration of high-fidelity dynamic optical arbitrary waveform generation," *Opt. Express* **18**(22), 22988–22995 (2010).
31. N. K. Fontaine, R. P. Scott, and S. J. B. Yoo, "Dynamic optical arbitrary waveform generation and detection in InP photonic integrated circuits for Tb/s optical communications," *Opt. Commun.* **284**(15), 3693–3705 (2011).
32. J. Yao, "Microwave photonics: Arbitrary waveform generation," *Nat. Photonics* **4**(2), 79–80 (2010).
33. M. H. Khan, H. Shen, Y. Xuan, L. Zhao, S. Xiao, D. E. Leaird, A. M. Weiner, and M. Qi, "Ultrabroad-bandwidth arbitrary radio frequency waveform generation with a silicon photonic chip-based spectral shaper," *Nat. Photonics* **4**(2), 117–122 (2010).
34. F. Parmigiani, T. T. Ng, M. Ibsen, P. Petropoulos, and D. J. Richardson, "Timing jitter tolerant all-optical TDM demultiplexing using a sawtooth pulse shaper," *IEEE Photon. Technol. Lett.* **20**(23), 1992–1994 (2008).
35. R. Ashrafi, M. Li, N. Belhadj, M. Dastmalchi, S. LaRochelle, and J. Azaña, "Experimental demonstration of superluminal space-to-time mapping in long period gratings," *Opt. Lett.* **38**(9), 1419–1421 (2013).
36. Y. Dai and J. Yao, "Arbitrary phase-modulated RF signal generation based on optical pulse position modulation," *J. Lightwave Technol.* **26**(19), 3329–3336 (2008).

1. Introduction

All-optical basic building blocks for photonic analog signal processing, such as optical real-time Fourier transformers [1], optical Hilbert transformers [2], optical differentiators [3], and optical integrators (OIs) [4], have been proposed and developed over the few past years. These building blocks provide a promising approach to perform signal processing functions at speeds beyond the capabilities of electronics. Besides their intrinsic interest in future ultrafast all-optical computing and information processing circuits, such devices have been used in a variety of applications including optical coherence tomography [1], instantaneous frequency measurement of broadband microwave signals [2], and to solve differential equations in the time-domain optically [5].

An OI is a linear photonic device capable of performing the time integral of an input optical signal [6]. A first-order OI outputs the first cumulative time integral of an input optical signal and is characterized by its ability to store optical energy. This feature has enabled the implementation of optical memory [7] and photonic bit counters [4] based on first-order OIs. In general, higher-order (e.g., second- or third-order) integrators capable of providing the

successive cumulative time integrals of the input signal are also key building blocks in processing circuits. While second-order OIs have also been successfully realized [8,9], there have been few studies on their potential applications.

In this paper, we propose and validate experimentally the use of second-order OIs to implement a novel photonic functionality, namely *time-delay to intensity mapping*. This process refers to the capability of controlling the optical amplitude (intensity) level of the signal generated at the output of a second-order OI by simply tuning the time delay between two consecutive optical pulses launched at the OI input. We propose using this mapping process for reconfigurable optical arbitrary waveform generation (OAWG), and provide proof-of-concept experimental demonstrations to validate our newly proposed OAWG scheme.

The remainder of this paper is organized as follows. In Section 2, we recall the functionality of OIs, introduce the operation principle of the proposed time-delay to intensity mapping process based on second-order OIs, and describe its application for OAWG. We present proof-of-concept experiments to validate our proposed OAWG concept in Section 3. In Section 4, the figure of merit parameters of the proposed OAWG approach are investigated. In Section 5, we discuss the design constraints of the proposed OAWG approach, including some comparisons with previously demonstrated OAWG techniques. Finally, in Section 6, we summarize the main conclusions of this work.

2. Operation principles

2.1. Background on OIs

Let us assume an optical signal defined as $x(t) \cdot \exp(j\omega_0 t)$, where $x(t)$ is the temporal complex envelope and ω_0 is the optical carrier frequency. If we launch this input signal into a first-order OI, the output signal $y_1(t) \cdot \exp(j\omega_0 t)$ will have a complex envelope that is proportional to the cumulative integral of the input complex envelope:

$$y_1(t) \propto \int_{t_1=-\infty}^t x(t_1) dt_1. \quad (1)$$

If instead, we launch the input signal into a second-order OI, the output complex envelope can be expressed as

$$y_2(t) \propto \int_{t_2=-\infty}^{t_2=t} \int_{t_1=-\infty}^{t_1=t_2} x(t_1) dt_1 dt_2, \quad (2)$$

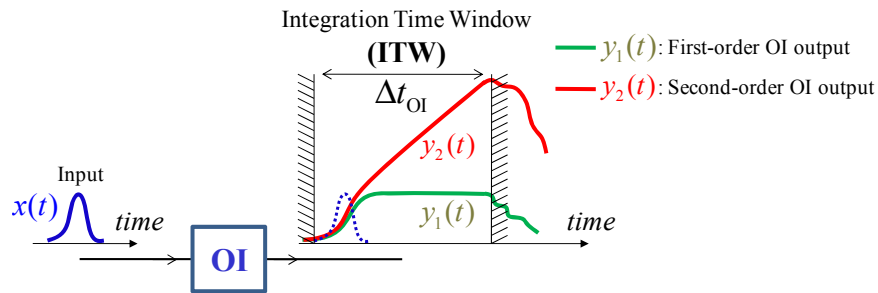


Fig. 1. Illustration of the first-order and second-order OI responses to a single Gaussian-like optical pulse. For better visualization of the first- and second-order OI outputs, $y_1(t)$ and $y_2(t)$ have been plotted with different peak amplitude scales.

which is the two-time cumulative integral of the input complex envelope. Figure 1 illustrates the time-domain output waveforms of the first- and second-order OIs in response to a single input Gaussian-like optical pulse.

OIs can be implemented using linear optical filters. In particular, first- and second-order OIs must provide temporal impulse responses of $h_1(t) \cdot \exp(j\omega_0 t)$ and $h_2(t) \cdot \exp(j\omega_0 t)$, respectively, where $h_1(t) \propto u(t)$, $h_2(t) \propto t \cdot u(t)$, and $u(t)$ is the unit-step function defined as $u(t) = 0$ for $t < 0$ and $u(t) = 1$ for $t \geq 0$ [10]. These ideal temporal impulse responses extend to infinity, thus requiring the use of a gain mechanism [11]. OIs can still be implemented using purely passive linear optical filters, most prominently single or concatenated low-loss optical resonant cavities [8,9]; in this case, the target device should emulate the ideal temporal impulse response over a limited, finite integration time window (ITW) only, e.g., with a duration of Δt_{OI} as illustrated in Fig. 1 [10]. These passive devices provide the time integral of an input optical waveform over this prescribed, finite time window.

2.2. Principle of time-delay to intensity mapping in OIs and application to OAWG

Consider a system comprising a cascade of two linear optical devices, a 1-tap time delay and a second-order OI, as shown in Fig. 2(a). Assume further that the 1-tap time delay generates a pair of π -phase shifted copies of the input pulse, separated by a prescribed time-delay τ ; we denote the time-delayed pair as $x(t) = s(t) - s(t - \tau)$, where $s(t)$ is the input pulse (complex envelope). The second-order optical integration of $x(t)$ can be approximately expressed as (see Fig. 2(a)):

$$\begin{aligned}
 y(t) &= \int_{t_2=-\infty}^{t_2=t} \int_{t_1=-\infty}^{t_1=t_2} [x(t_1)] dt_1 dt_2 \\
 &= \int_{t_2=-\infty}^{t_2=t} \int_{t_1=-\infty}^{t_1=t_2} [s(t_1) - s(t_1 - \tau)] dt_1 dt_2 \approx \begin{cases} \alpha \cdot t & 0 < t < \tau \\ \alpha \cdot \tau & t > \tau \end{cases}, \quad (3)
 \end{aligned}$$

where α is the slope of the temporal impulse response of the second-order OI. Recall that the output signal variation — a temporal ramp reaching a certain peak amplitude level, which keeps constant following the arrival of the second optical pulse — is a direct result of the π phase shift between the two input pulses. Clearly, when the time delay τ is increased, the peak amplitude level of the corresponding signal at the OI output increases linearly with a slope defined by α . This linear relation between the time delay and the output amplitude level implements the predicted **time-delay to intensity mapping**. Also notice that the output signal intensity depends on the square of the input time delay.

Based on the *time-delay to intensity mapping*, we propose a general architecture for OAWG as illustrated schematically in Fig. 2(b). We now consider the OAWG scheme, having an N -tap arrayed time-delay (ATD) in the system, as illustrated in Fig. 2(b). If the input to the second-order OI is an N -tap ATD as opposed to a 1-tap ATD, then according to Eq. (3), each tap (n) at the corresponding point of the time-domain output [$n = 1, 2, \dots, N$ where N is the number of taps], can increase or decrease the intensity level by an amount of $(\alpha \cdot \tau_n)^2$. In particular, the signal intensity at a given temporal point (n) is increased or decreased with respect to the previous point ($n-1$), depending on the starting phase (zero or π) of the tap (n) with respect to tap ($n-1$). In general, a complex (amplitude and phase) variation from point-to-point of the time-domain output optical waveform could be achieved by simply having more levels of control on the starting phase of each tap.

The taps of the ATD are temporally separated with a fixed time-delay (T), as shown in Fig. 2(b). The temporal resolution of the proposed OAWG is thus given by $1/T$ (samples/s) and the temporal duration of the generated output optical waveform is $N \cdot T$. The maximum temporal duration of the waveform, $N \cdot T$, is ultimately constrained by the ITW of the second-

order OI, i.e., $N \cdot T < \Delta t_{OI}$. As illustrated in Fig. 2(b), if necessary, the staircase-like output of the OI (dotted red curve) can be converted to a desired smooth output waveform (solid red curve) by applying a low-pass filtering.

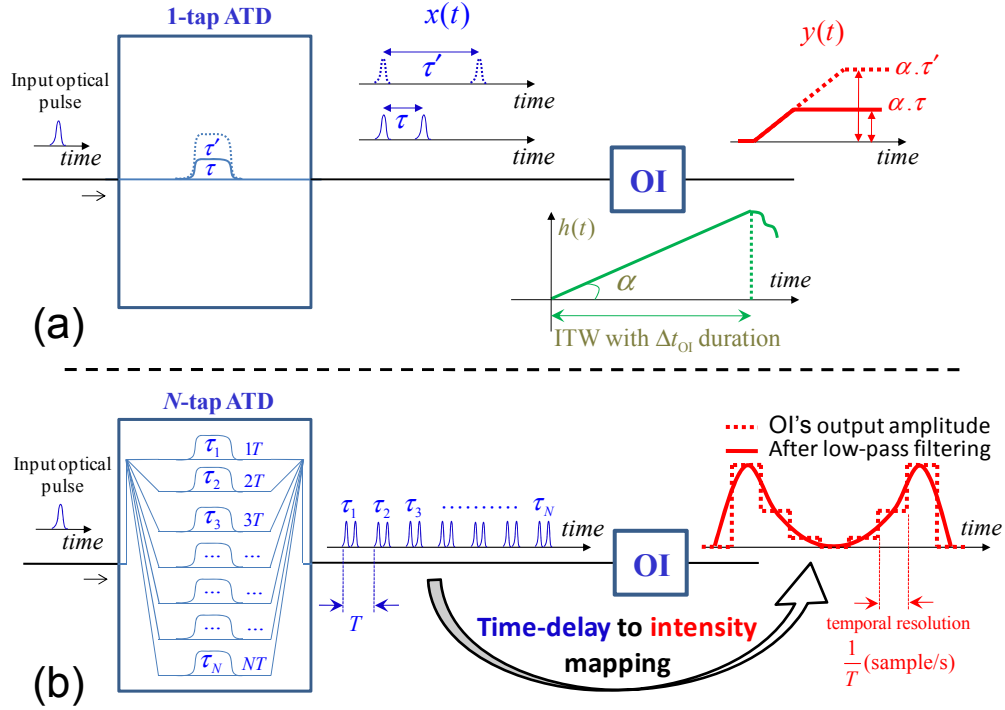


Fig. 2. (a) Operation principle of the time-delay to intensity mapping process in a second-order OI. (b) General architecture of the proposed OAWG approach based on the time-delay to intensity mapping process using an N -tap ATD.

3. Experimental results

We have implemented the following system configuration in order to validate the proposed OAWG approach. An 8-tap ATD ($N = 8$) with $T = 0.5$ ps delay between the taps has been implemented using a benchtop programmable optical filter (POF), here a Finisar Waveshaper 1000-S. This translates to an output temporal sampling rate of 2,000 Gsamples/s over a temporal duration of 4 ps. The frequency response of the POF has been programmed to obtain the corresponding ideal time-domain impulse response of an 8-tap ATD. The frequency bandwidth over which the ATD is realized is equal to the operation bandwidth of the employed POF, i.e. from 1527.4nm to 1567.5nm (~ 5 THz bandwidth). The frequency transfer function of an 8-tap ATD can be expressed as

$$H_{\text{ATD}}(\omega) = \sum_{n=1}^8 e^{-j\varphi_n} \cdot \left\{ e^{-j\omega(n \cdot T)} - e^{-j\omega(n \cdot T - \tau_n)} \right\}, \quad (4)$$

where φ_n is the starting phase (zero or π) of the n th tap. The frequency resolution of the POF to synthesize the transfer function H_{ATD} is ~ 10 GHz. Both phase and amplitude of the H_{ATD} should be programmed in the POF to implement the target 8-tap ATD.

Note that due to the lack of a proper ATD device, we have employed this frequency-domain approach to implement the equivalent of a time-delay array system; clearly, this is not the most efficient way to realize the ATD but should be sufficient to provide a conceptual

proof of our proposed ideas. In particular, the limited frequency resolution (10 GHz for the Finisar Waveshaper 1000-S) of the POF greatly restricts the maximum delay range to $N \cdot T \sim 4$ ps. This is because based on Fourier transformation theory, the minimum resolution/features of a linear filter in the frequency domain set the large features in the time domain and the maximum temporal duration of the filter impulse response. When we configure the POF to implement a time-delay functionality, the minimum step size in the frequency domain (i.e., 10 GHz) of the POF, affects the amplitude (and quality) of the output pulses from the time-delay system when we increase the delay. For example, the frequency transfer function $H_{\text{ATD}}(\omega)$ of a 1-tap time delay system is proportional to $\sin(0.5\omega\tau)$, where τ is the delay between the two pulses at the output of the time delay system in response to one single pulse. The frequency transfer function $H_{\text{ATD}}(\omega)$ has several spectral resonance dips at the zero points of the function $\sin(0.5\omega\tau)$. If we want to increase the delay, the bandwidth of the spectral dips, to be realized by the POF, will become narrower and require a higher spectral resolution to be synthesized. Therefore, if the point-by-point frequency resolution of the POF is not sufficient to synthesize the required spectral dips with enough depth, the two output pulses from the POF will have considerably different amplitudes. According to our measurements, for our POF, if we limit the maximum delay range to ~ 4 ps, the amplitude difference for the output pulses from the POF-based ATD is below 10%. As illustrated in Fig. 2(b), for an optimized performance and integrated implementation, the ATD should be realized using a multi-arm interferometer structure with individual time-delay control in each tap.

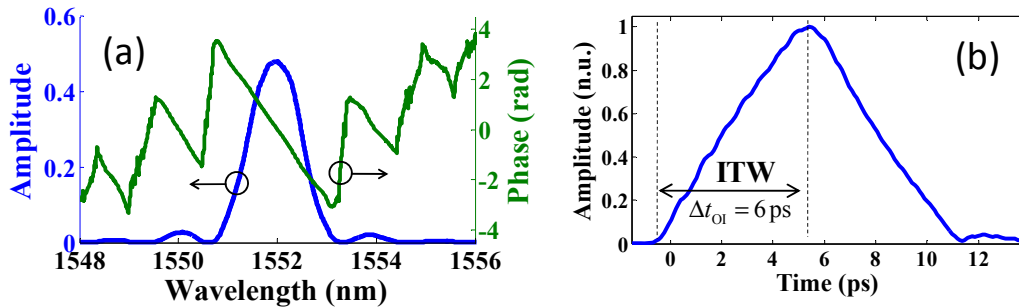


Fig. 3. The measured spectral (a) and temporal impulse (b) responses of the implemented second-order OI.

A second-order OI, with an ITW duration of $\Delta t_{\text{OI}} = 6$ ps, has also been implemented using a second POF (Finisar Waveshaper 4000-S). In a practical setup, integrated OIs with significantly longer ITWs could be readily implemented using Bragg grating (BG) devices or micro-ring resonators [8,9]. Figure 3 shows the measured spectral and temporal impulse responses of the second-order OI (details of the measurement technique are provided below). Notice that as demonstrated in [10], the output signal of the OI is not necessarily zero outside the ITW, even when the impulse response is forced to be zero. If necessary, additional time-gating, i.e., temporal modulation, may be used to extract the valid integrated signal, i.e., the target generated optical waveform. In particular this is important when the input pulse has a high repetition rate, which may lead to crosstalk between the target waveform and the unwanted waveform outside the ITW. This becomes an issue of setting the input repetition rate parameters so that to have no overlap/crosstalk, i.e., the maximum input repetition rate has to be the inverse of the entire OI output duration. In our experiments, since the repetition rate of the input pulse is low enough (i.e. 20MHz), we did not need to employ any time-gating process and the reported plots only show the generated output waveform within the ITW. As shown in Fig. 3(b), the temporal impulse response of our second-order OI is not zero outside the ITW. We have synthesized this symmetric profile for the OI's temporal impulse response, since we have observed that this choice translates into a better extinction ratio (*ER*) between

the target optical waveform and the subsequent undesired part of the signal (see the Appendix for more details).

Figure 4 shows the experimental setup for time-domain characterization of the synthesized optical waveforms at the output of the OAWG system. The characterization principle is based on Fourier-transform spectral interferometry (FTSI) [12], in which the spectral amplitude and phase profiles are retrieved and used to obtain the complex temporal waveform at the output of the OAWG system. In the FTSI characterization setup, a copy of the input pulse is used as the reference signal to create a spectral interference with the output of our OAWG system as illustrated in Fig. 4 [12]. The input optical pulse is a nearly transform-limited Gaussian-like pulse generated directly from a passively mode-locked fiber laser (MLL) (FPL, CALMAR Inc.) with a repetition rate of 20 MHz. The spectra of the output waveform and the reference pulse as well as the resulting spectral interferogram are measured using an optical spectrum analyzer (OSA). All these measurements are employed for numerical reconstruction of the OAWG system's output waveform using a conventional FTSI algorithm [12]. In the reference arm, a tunable delay line (TDL) is used to tune the time spacing between the signals in the two arms (reference pulse and output waveform). The delay between the output waveform and the reference pulse was chosen to be around 30 ps, which is large enough to separate temporally the output waveform from the input pulse. Moreover, it is small enough to identify properly the FTSI's spectral interferogram features according to the OSA's spectral resolution.

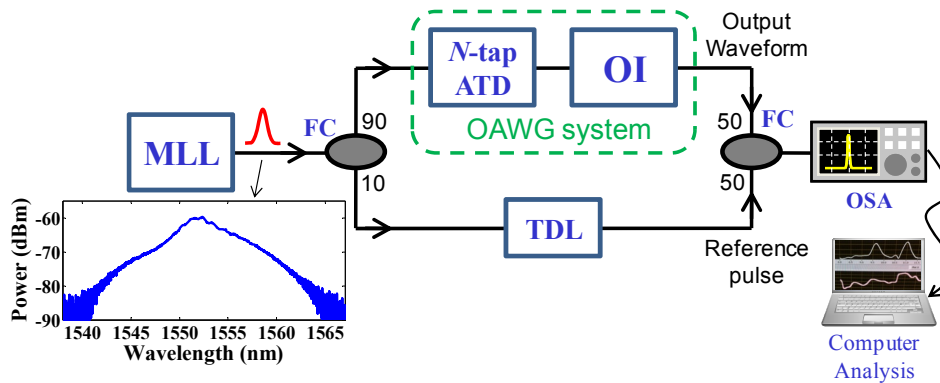


Fig. 4. Experimental setup for time-domain output measurement of the implemented OAWG system based on FTSI method. MLL: mode-locked laser; OSA: optical spectrum analyzer; FC: fiber coupler, TDL: tunable delay line.

The MLL produces pulses with an FWHM time width of ~ 420 fs centered at 1552 nm. Accordingly, the central wavelength of the second-order OI is implemented at this same wavelength. The time-delay vector of the ATD is represented by $\tau = [\tau_1 \pm \tau_2 \pm \tau_3 \pm \tau_4 \pm \tau_5 \pm \tau_6 \pm \tau_7 \pm \tau_8]$ where τ_i is the time-delay between the two π -phase-shifted pulses in each tap and its sign defines its starting phase with respect to the previous tap. Note that the low-pass filtering illustrated in Fig. 2(b) is not required since the smoothing process is carried out by the input pulse width being on the order of $T = 0.5$ ps. Our results clearly prove that by tuning the value of the time-delays τ_i in the ATD, one can synthesize arbitrary waveforms with the desired temporal shape. In particular, we target the following optical waveforms: (a) triangular pulse with equal rising and falling times, (b) triangular pulse with slow rising time and fast falling time, (c) Triangular pulse with fast rising time and slow falling time, (d) flat-top pulse, (e) convex parabolic pulse, and (f) concave parabolic pulse. Table 1 presents the time-delay values of each tap in the ATD that are needed for generation of each of these optical waveforms.

Table 1. The values of the tuned time-delay vector for generation of the optical waveforms shown in Fig. 5.

	τ_1	τ_2	τ_3	τ_4	τ_5	τ_6	τ_7	τ_8
(a)	+ 100 fs	+ 100 fs	+ 100 fs	+ 100 fs	100 fs	100 fs	100 fs	100 fs
(b)	+ 40 fs	-280 fs						
(c)	+ 280 fs	-40 fs	-40 fs	-40 fs	-40 fs	-40 fs	-40 fs	-40 fs
(d)	+ 100 fs	0	0	0	0	0	0	-100 fs
(e)	+ 280 fs	+ 200 fs	+ 120 fs	+ 40 fs	-40 fs	-120 fs	-200 fs	-280 fs
(f)	+ 270 fs	-150 fs	-90 fs	-30 fs	+ 30 fs	+ 90 fs	+ 150 fs	-270 fs

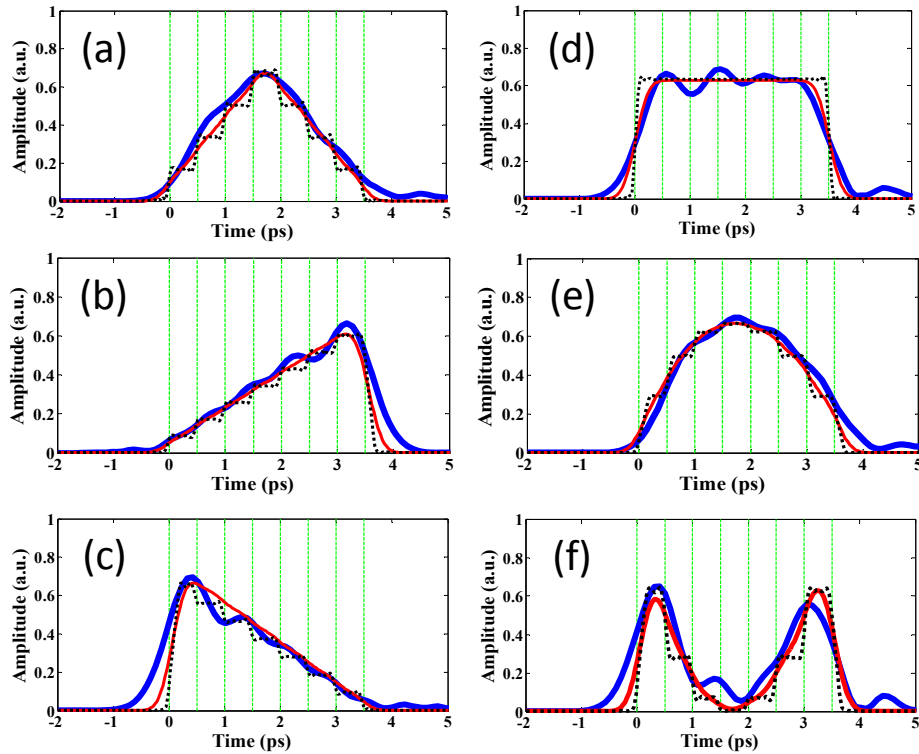


Fig. 5. Experimentally measured (solid blue curves) and simulated (solid red curves) waveforms generated at the output of the implemented OAWG system. The simulated temporal impulse response of the OAWG system is also shown by a dotted black curve. The OAWG system has $N = 8$ taps with $T = 0.5$ ps delay between the taps. The time-delay vector has been tuned for synthesizing the following optical waveforms; (a) triangular pulse with equal rising and falling times, (b) triangular pulse with slow rising time and fast falling time, (c) Triangular pulse with fast rising time and slow falling time, (d) flat-top pulse, (e) convex parabolic pulse, and (f) concave parabolic pulse. The time-delay vectors are presented in Table 1 for each waveform generation case.

The experimentally recovered time-domain amplitude profiles at the output of the OAWG system are shown in Fig. 5, along with the simulated temporal impulse response and output waveform from the OAWG system. The simulated temporal impulse response of the OAWG system, i.e., the dotted black curves in Fig. 5, was obtained by convolving the ideal temporal impulse of an 8-tap ATD (with the values of the time-delay vector given in Table 1) and an ideal ramp temporal impulse response for the OI. This ideal temporal impulse response of the OAWG system was then numerically convolved with an input Gaussian pulse with 420 fs FWHM time width to obtain the simulated output waveform, i.e., the solid red curves in Fig. 5. There is a fairly good agreement between the experimental and numerically simulated results. Moreover, in the six examples considered, the obtained temporal waveforms at the system output closely follow the corresponding ideal impulse response that is predicted through the proposed time-delay to intensity mapping process.

4. OAWG system performance analysis

The performance of the OAWG systems is evaluated by two figures of merit: the time-bandwidth product (*TBP*) and amplitude dynamic range (*ADR*) for the generated output waveform. In this section, we analyze these two figures of merit for the proposed OAWG scheme.

4.1. Time bandwidth product (*TBP*)

The *TBP* characterizes the performance of the waveform generation process in terms of providing the maximum temporal duration and spectral bandwidth of the output waveform, and is expressed as

$$TBP = \Delta t_{WG} \times BW_{WG} , \quad (5)$$

where Δt_{WG} and BW_{WG} are estimates of the maximum temporal duration and frequency bandwidth of the waveform generation process, respectively. As explained in the operation principle of the proposed OAWG system in Section 2.2, Δt_{WG} and BW_{WG} are essentially determined by the temporal separation (T) and the number (N) of taps in the ATD:

$$\Delta t_{WG} = N \cdot T , \quad (6)$$

$$BW_{WG} \approx 1/T , \quad (7)$$

Therefore, similarly to previous OAWG techniques [13–16], the *TBP* of our proposed OAWG approach is determined by the number of taps in the system, i.e.,

$$TBP \approx N . \quad (8)$$

The OI device in the proposed OAWG system should provide an ITW with a duration of Δt_{OI} and an effective spectral bandwidth of BW_{OI} , both larger than those defined in Eqs. (6) and (7):

$$\Delta t_{OI} > \Delta t_{WG} , \quad (9)$$

$$BW_{OI} > BW_{WG} , \quad (10)$$

To be more concrete, the OI should provide a spectral response close to the ideal integrator response within a bandwidth larger than the sampling rate of the ATD ($1/T$). Figure 6 shows a numerical analysis of the impact of reducing the OI's bandwidth on the output temporal waveform in terms of generating a target value at each output temporal point. In this analysis, we consider the same OAWG system parameters as for the above experimental implementation. Only two amplitude levels are considered for the target output waveform to be synthesized using a time-delay vector of $\tau = [+ 100\text{fs} \ -100\text{fs} \ 0 \ 0 \ + 100\text{fs} \ + 100\text{fs} \ -100\text{fs}$

–100fs]. Figure 6(a) shows the OI's spectral response in the ideal case with no bandwidth limitation and also for three different cases of OIs with reduced bandwidths. A low-pass Gaussian filter with FWHM spectral width of 3.7 THz, 1.85 THz and 0.92 THz has been applied to the ideal OI's response to synthesize the spectral response of the OIs for the three cases of Case 1, Case 2 and Case 3, respectively, shown in Fig. 6(a). The corresponding generated output waveform for each case is shown in Fig. 6(b). We can see at the eight output temporal points, shown with the green arrows, the amplitude deviations from the target levels are increased when the OI's bandwidth is decreased. In particular, the OI in Case 1 has a response very close to the ideal case within a bandwidth of $1/T = 2$ THz (or ~ 16 nm centered at 1552 nm). Correspondingly, the synthesized amplitude levels at the eight output temporal points for Case 1 is very close to the target amplitude levels. Clearly by having more reduction on the OI's bandwidth as for Case 2 and Case 3, the synthesized amplitude levels start to have more deviations from the target levels at each output temporal point. This suggests that the OIs in Case 2 and Case 3 may not be suitable for the waveform generation process with a sampling rate of $1/T = 2,000$ Gsamples/s, i.e., they are better suited for lower sampling rates.

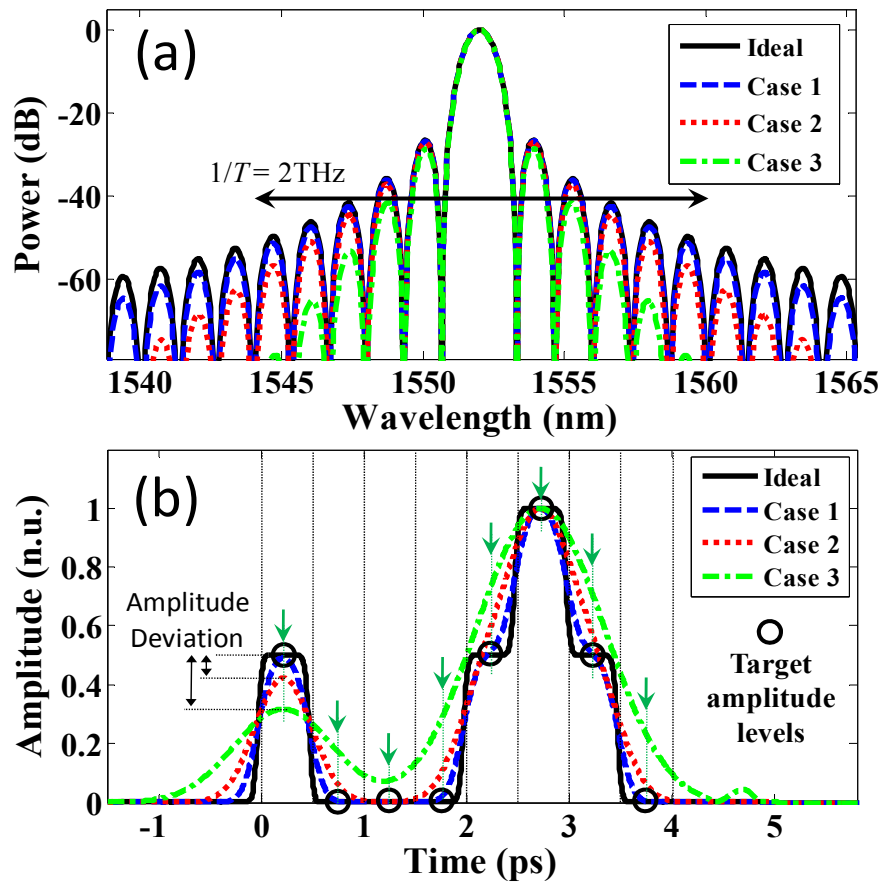


Fig. 6. A numerical analysis for the spectral bandwidth requirement of the OI in the proposed OAWG technique. (a) OI's spectral response in ideal case with no bandwidth limitation and also for three different cases of OIs with reduced bandwidths. (b) The corresponding generated output waveform for each case. A low-pass Gaussian filter with FWHM spectral width of 3.7THz, 1.85THz and 0.92THz has been applied to the ideal OI's response to synthesize the spectral response of the OIs for the three cases of Case 1, Case 2 and Case 3, respectively.

Experimental implementations of second-order OIs based on BG devices and micro-ring resonators have been reported with ITWs and spectral bandwidths in the range of tens of ps and hundreds of GHz, respectively [8,9]. This implies that the proposed OAWG approach can be readily implemented based on integrated-waveguide/fiber-optics platforms to provide waveform generation at hundreds of Gsamples/s over temporal windows up to a few tens of ps. Realistic advances on OI technologies can be expected in the near future to improve further this performance.

ATD devices based on various optical technologies such as micro-electro-mechanical-system (MEMS) [17], fiber-optics [18,19], and integrated-waveguides [20–27] have been developed, mostly for microwave phased array antenna applications. For the purpose of the OAWG approach in this work, ATDs based on integrated-waveguide solutions are preferred. This would enable a more accurate control of the waveguide lengths, which in turn would lead to higher OAWG temporal resolutions (sampling rate). In particular, in addition to being a more compact solution than alternative ATD technologies, integrated-waveguide optical delay lines can provide far better precisions than that required for hundreds of Gsamples/s OAWG (i.e., sub-ps-resolution). The accuracy on the waveguide length control is typically set by fabrication processing variations or the lithography mask quantization [28]. Current photonic integration technologies provide either sub-90-nm or sub-10-nm waveguide length control resolutions, depending on whether optical or electron-beam lithography technologies are used [29]. These length control resolutions directly translate into the possibility of achieving sub-fs temporal resolutions. However, note that as implied by Eqs. (9) and (10), for development of an integrated OAWG with higher temporal resolutions, e.g., several Tsamples/s, integrated OI devices with the corresponding large spectral bandwidths (several THz) will need to be developed.

4.2. Amplitude dynamic range (ADR)

A figure of merit referred to as *ADR* is used to estimate the amplitude resolution offered by the system, namely the precision with which a prescribed, target amplitude level can be approached at each output temporal point. Note that in our analysis of the *ADR* for our proposed OAWG scheme, the OI spectral bandwidth condition presented in Eq. (10) is assumed to be satisfied. Figure 7 shows an illustration of some basic parameters used for estimating the *ADR* in the proposed OAWG scheme.

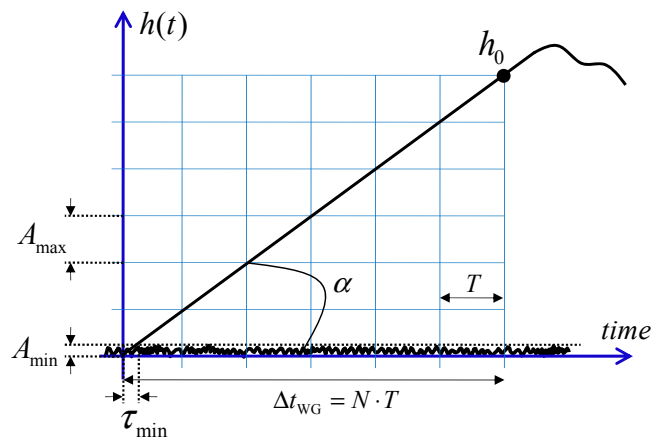


Fig. 7. An illustration of some basic parameters defined on the temporal impulse response of the OI, for obtaining estimates of the *ADR* in the proposed OAWG scheme. For better visualization of the *ADR* estimation method, the impulse response ripples of the OI has been illustrated separately from the ramp profile.

Theoretically, by assuming that there are no ripples in the impulse response of the OI, the time-delay between the two pulses in each tap can be tuned in a continuous manner. However, in practice, the OI's temporal impulse response will exhibit a finite signal-to-noise ratio (SNR), defined as the ratio between the peak value of the impulse response and the maximum peak-to-peak value of the ripples. Note that in Fig. 7, for better visualization of the ADR estimation method, the ripples have been illustrated separately from the impulse response of the OI. In this case, the time-delay tuning should have a minimum step size, denoted by τ_{min} in Fig. 7, so that to ensure the amplitude level increase can be distinguished above the noise level. Correspondingly, the amplitude tuning will have a minimum step size, denoted by A_{min} . From Fig. 7, these parameters can be expressed as

$$A_{min} = \frac{h_0}{\sqrt{SNR}}, \quad (11)$$

$$\tau_{min} = \frac{A_{min}}{\alpha}, \quad (12)$$

where h_0 is the maximum amplitude sweeping range for the whole time-window duration of $N \cdot T$. The amplitude sweeping range within the time-window of one tap is $A_{max} = h_0/N$. Therefore, the ADR of the OAWG system can be estimated as

$$ADR = \frac{A_{max}}{A_{min}} = \frac{\sqrt{SNR}}{N}, \quad (13)$$

Equation (13) reveals a trade-off between the achievable amplitude and temporal resolutions in the proposed OAWG scheme. In particular, let's assume a fixed temporal duration of Δt_{WG} , no spectral bandwidth limitation in the OI device and a fixed SNR in the OAWG system. By increasing the number of taps (N), the temporal resolution ($1/T$) of the waveform generation process will increase. However, this will cause a degradation on the OAWG amplitude resolution by decreasing the ADR parameter. Therefore, for a fixed number of taps, the only way to increase the amplitude resolution (ADR) is to improve the SNR of the system. This can be achieved to some extent by increasing the slope (α) of the temporal ramp impulse response of the OI device, i.e., equivalent to increasing h_0 in Fig. 7. Note that for a passive OI with a fixed ITW, the value of h_0 (or α) depends on the peak power spectral response of the device [10].

5. Discussion

Concerning previously demonstrated OAWG approaches, solutions based on direct electro-optic modulation offer the capability of generating arbitrary waveforms with extremely large TBP s in a reconfigurable fashion; however, they require the use of complex, multi-frequency implementations to achieve time resolutions beyond the limited frequency bandwidth of the electro-optic modulation processes [30,31]. To overcome this important drawback, different photonics-based OAWG approaches have been proposed and implemented mainly based on two linear optical pulse shaping approaches: (1) direct linear spectral filtering, e.g., using integrated silicon photonic spectral shapers [32,33], fiber Bragg gratings (BGs) [34] and long period gratings [35], non-uniform delay line filtering [36], or bulk-optics components [13–15], and (2) temporal coherence synthesization [16]. However, these solutions generally suffer from either complex bulk-optics implementations, with limited integration with fiber-optics and integrated-waveguide systems [13–15], or very limited capabilities for tuning the shape of the generated waveforms [16,32–36].

The OAWG concept suggested here, using *time-delay to intensity mapping* in an OI, offers the unique ability of arbitrarily tuning the amplitude (or intensity) of the generated optical

waveform at each temporal point, see Fig. 2(b), without the stringent bandwidth limitations of a direct electro-optic approach, e.g., with resolutions into the sub-picosecond regime. Additionally, the proposed scheme could be implemented in integrated-waveguide or fiber-optics platforms. Point-by-point intensity tuning is achieved by changing the input time-delays, i.e., the values of τ_i in an ATD, a functionality that can be readily implemented in integrated-waveguide configurations [20–27]. Each input time-delay τ_i is linearly mapped into a desired corresponding output amplitude level based on the *time-delay to intensity mapping* process in a second-order OI. This device can be practically implemented using BGs (fiber or waveguide) or micro-ring resonators [8,9]. Thus, in addition to its fundamental, intrinsic interest, the proposed concept shows great promise for development of ultra-high-speed reconfigurable OAWG platforms in integrated-waveguide formats.

The proposed OAWG scheme requires a tight control of unintentional phase variations between the different taps; nonetheless, the needed phase control is at least similar to the typical requirements in other reported OAWG approaches [13–16], and in this regard an integrated-waveguide implementation of the system is preferred. In the proposed OAWG approach, for generation of amplitude-only waveforms, two levels of control (zero or π) on the starting phase of each tap is required. As described in Section 4.1, current integrated photonic fabrication facilities can provide a waveguide length control as good as sub-10-nm precision [28,29]. A length control precision of 10 nm (in silicon) translates into ~ 0.1 fs time-delay control and a corresponding $\sim \pi/23$ phase level control between different taps of the ATD structure, which is clearly sufficient for the purpose of the OAWG approach proposed in this work.

Another important practical consideration concerns the fact that the performance of the waveform generation process in the proposed approach, evaluated in the form of *TBP*, directly depends on the number of taps in the system. This constraint is again similar to that found in previous OAWG approaches [13–16]. To increase the number of taps (to achieve a higher *TBP*), passive losses of the input $1 \times N$ splitter and output $N \times 1$ combiner in the ATD device should be optimized.

6. Summary

We have proposed and experimentally demonstrated a novel photonic process, time-delay to intensity mapping, using a second-order OI. In particular, we have shown how linear intensity control can be achieved at the output of a second-order OI by simply setting the time-delay between two π -phase shifted optical pulses launched into the OI. This mapping process has been shown to be particularly interesting for OAWG. An scheme has been proposed capable of providing precise point-by-point intensity control of the optical waveform generated at the output of a second-order OI by simply tuning the input time-delay vector of an ATD system. We anticipate that customized complex optical temporal waveforms with femtosecond range temporal resolutions could be synthesized using available photonic technologies for implementation of the ATD and OI devices. OAWG at 2,000 Gsamples/s has been demonstrated using the proof-of-concept experimental setup reported here. A critical limitation of the proposed OAWG approach is that the total duration of the generated waveform is constrained by the duration of the OI's temporal impulse response. We anticipate that OIs with customized impulse response durations approaching the nanosecond range could be potentially implemented using practical fiber/integrated-waveguide micro-ring resonators or BG structures.

Appendix

In this Appendix, we show numerically the impact of choosing a symmetric ramp temporal impulse response for the OI (as illustrated in Fig. 8(b)) to achieve a higher *ER* for the output waveform, as compared to a non-symmetric ramp response, where it is forced to be zero

outside the ITW (as illustrated in Fig. 8(a)). In this numerical analysis, we consider the case of flat-top pulse generation [Fig. 5(d)].

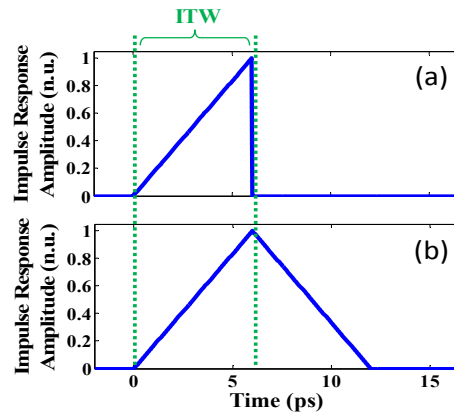


Fig. 8. Two alternative impulse response profiles of a passive second-order OI.

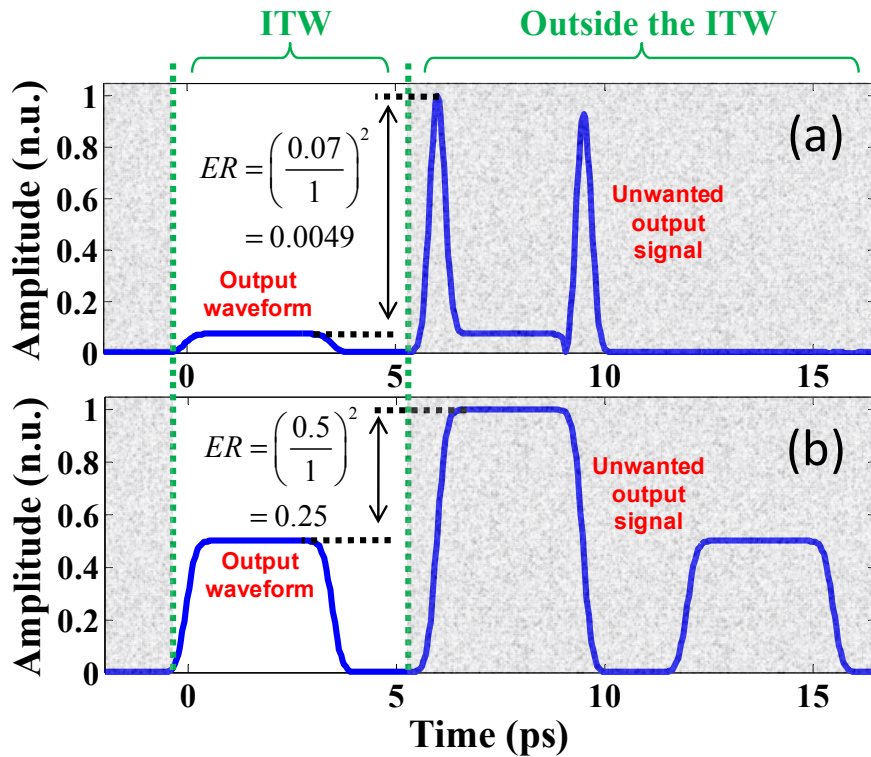


Fig. 9. The numerically simulated total signal at the output of the proposed OAWG scheme, for the two cases of the OI's impulse response profiles shown in Fig. 8(a), (b). The total output signal includes the target output waveform (i.e. the flat-top pulse) within the ITW, and the output signal outside the ITW. The estimated ER s are given in each case.

As mentioned in Section 3, the output signal of the OI is not necessarily zero outside the ITW. The amplitude of the output signal outside the ITW depends on the OI's impulse response profile. Fig. 9 shows the simulated output waveform (flat-top pulse) within the ITW and the unwanted signal outside the ITW for the two OI impulse response profiles shown in

Figs. 8(a) and 8(b). The *ER* is obtained as the ratio between the peak power of the target output waveform to the peak power of the unwanted output signal. As mentioned in Section 3, the unwanted output signal outside the ITW can be eliminated by using a time-gating technique. However, for the proof of concept experiments reported here, we did not employ any time-gating process and therefore, an unwanted signal exists outside of the ITW, affecting the waveform characterization. As shown in Fig. 9, the estimated *ERs* for the two cases of impulse response profiles in Figs. 8(a) and 8(b), are 0.0049 and 0.25, respectively. This clearly shows that the *ER* can be considerably improved (~ 50 times) by choosing the symmetric ramp temporal impulse response for the OI in the proposed OAWG approach.

Acknowledgments

This research was supported by the Natural Sciences and Engineering Research Council of Canada (NSERC).